Enhanced Particle Filtering for Bearing Remaining Useful Life Prediction of Wind Turbine Drivetrain Gearboxes

Fangzhou Cheng, *Member, IEEE*, Liyan Qu, *Senior Member, IEEE*, Wei Qiao, *Senior Member, IEEE*, and Liwei Hao, *Senior Member, IEEE*

***Abstract*—Bearing is the major contributor to wind turbine gearbox failures. Accurate remaining useful life prediction for drivetrain gearboxes of wind turbines is of great importance to achieve condition-based maintenance to improve the wind turbine reliability and reduce the cost of wind power. However, remaining useful life prediction is a challenging work due to the limited monitoring data and the lack of an accurate physical fault degradation model. The particle filtering method has been used for the remaining useful life prediction of wind turbine drivetrain gearboxes, but suffers from the particle impoverishment problem due to a low particle diversity, which may lead to unsatisfactory prediction results. To solve this problem, this paper proposes an enhanced particle filtering algorithm in which an adaptive neuro-fuzzy inference system is designed to learn the state transition function in the fault degradation model using the fault indicator extracted from the monitoring data; a particle modification method and an improved multinomial resampling method are proposed to improve the particle diversity in the resampling process to solve the particle impoverishment problem. The enhanced particle filtering algorithm is applied successfully to predict the remaining useful life of a bearing in the drivetrain gearbox of a 2.5 MW wind turbine equipped with a doubly-fed induction generator.**

***Index Terms*—Enhanced particle filtering (EPF), gearbox, prediction, remaining useful life (RUL), wind turbine.**

NOMENCLATURE

n	Order of Markov model.
x_k	Actual value of state at time k.
z_k	Measurement of state at time k.
v_k	Measurement noise.
$\hat{x}_{k+1}^i$	State of the i^{th} particle at time k+1.
f_k	The nonlinear state transition function in the fault degradation model.
u_k	Gaussian white noise in the state transition function.
N	Number of particles.
$\hat{x}_{k+1}$	Estimated value of state at time k+1.
w_k^i	Weight of the i^{th} particle at time k.
$\delta(\bullet)$	Dirac delta function.
N_{k+1}^i	Number of the resampled particles whose states are equal to $\hat{x}_{k+1}^i$.
N_{eff}	Effective number of particles.
N_{thres}	Threshold used to perform resampling.
E_l	Set containing the states of small-weight particles.
E_h	Set containing the states of large-weight particles.
W_{th}	Threshold for separating large- and small-weight particles.
$\bar{W}$	Weights of particles sorted in the descending order.
x_{kh}^t	State of a particle in E_h.
x_{kl}^s	State of a particle in E_l.
x_{km}^s	State of a modified small-weight particle.
w_{kl}^s	Weight of x_{kl}^s.
w_{kh}^t	Weight of x_{kh}^t.
N_h	Number of particles contained in E_h.
N_l	Number of particles contained in E_l.
X_k'	Set containing the states of the original large-weight particles and modified small-weight particles.
x'^i_k	State of the i^{th} resampled particle stored in X_k'.
N'^i_k	Number of the resampled particles whose states are equal to x'^i_k.
$\bar{X}_k^i$	Set containing the states of new resampled particles generated from x'^i_k.
Δh_j	Deviation of the state of a new resampled particle.
λ	Decentralization parameter.
$\bar{X}_k$	Set containing the states of all the new resampled particles.
$\hat{z}_{k+m}$	Predicted measurement of state at time k+m.
T_p	Prediction period.
$e_{1,2}$	Metrics for evaluating the particle filtering performance.
N_s	Number of experiments for RUL prediction.
T_m	Monitoring period.
$\hat{x}_k^{(u)}$	State predicted at time k for the u^{th} experiment.

Manuscript received November 15, 2017; revised May 14, 2018 and July 5, 2018; accepted August 2, 2018. This work was supported in part by the Office of Energy Efficiency and Renewable Energy (EERE), U.S. Department of Energy, under Award Number DE-EE0006802, and in part by the U.S. National Science Foundation under Grants ECCS-1308045 and CMMI-1663562.

F. Cheng is with the System Sciences Laboratory, Palo Alto Research Center, Palo Alto, CA 94304 USA (e-mail: fangzhou.cheng@parc.com).

L. Qu and W. Qiao are with the Power and Energy Systems Laboratory, Department of Electrical and Computer Engineering, University of Nebraska—Lincoln, Lincoln, NE 68588-0511 USA (e-mail: wqiao3@unl.edu; lqu2@unl.edu).

L. Hao is with the GE Global Research, Niskayuna, NY 12309 USA (e-mail: hao1@ge.com).

I. INTRODUCTION

Gearbox failure is one of the leading reliability issues in doubly-fed induction generator (DFIG)-based wind turbines [1]-[3]. According to a report [4], gearbox is the leading contributor to the downtime of both onshore and offshore

DFIG-based wind turbines ranging from 500 kW to 5 MW. Moreover, the replacement costs for drivetrain gearboxes are high. For instance, replacing the gearbox in the drivetrain of a 5 MW wind turbine can cost more than $600,000 [5]. According to another survey [6], the majority of wind turbine gearbox failures are caused by bearings. Among various bearing failures, axial cracks on the bearings in the high-speed stages (HSSs) are the leading causes. Therefore, to reduce the downtime and maintenance costs of DFIG-based wind turbines, it is highly desired to detect bearing faults and predict the remaining useful life (RUL) of the bearings in the gearboxes as early as possible. In this way, the traditional scheduled maintenance can be replaced by condition-based maintenance (CBM) so that the faulty components can be repaired timely to prevent further damages of the drivetrains or catastrophic failures of the wind turbines [7].

The CBM is gaining growing interests for improving the reliability of complex systems in industrial, military, and other applications. The CBM relies on the assessment of the health condition of the system using a program consisting of condition monitoring, feature extraction, fault diagnosis, fault prognosis, maintenance action, etc. Fault prognosis is a key part of the CBM and is performed after fault diagnosis to predict the future progress and propagation of the fault and the RUL of the system being monitored. However, unlike fault diagnosis for drivetrain gearboxes of wind turbines, which has been widely studied by academic and industry [8]-[19], fault prognosis and RUL prediction are relatively new domains.

The major methods for fault prognosis and RUL prediction can be generally categorized into model-based (or physics-based) methods and data-driven methods. The model-based methods assume that an accurate physical degradation model can be obtained to predict the development of a failure process [20]. Different model-based methods have been proposed for RUL prediction [21], [22]. However, it is usually difficult to build accurate physical degradation models for complex real-world systems; and the identification of model parameters requires extensive experiments and empirical data. In the data-driven methods, the raw monitoring data is transformed into relevant information from which the degradation models are derived without concerning about the physics of the system degradation processes [23]. The data-driven methods mainly use statistical or artificial intelligence (AI) tools to learn the degradation processes and predict the future health states of the systems. A data-driven method typically consists of two phases: learning the fault degradation process in the first phase and then predicting its future state in the second phase. Different data-driven methods have been developed and successfully applied for RUL prediction [24]-[26]. However, it is not easy to explain the physical meaning of the results obtained from the data-driven models. Moreover, it may require significant computational resources to train the AI algorithms and process the data [27].

Particle filtering (PF) is a widely-used method to estimate and update the states and parameters in model-based methods based on the concept of sequential importance sampling (SIS) and Bayesian theory [28]. In the PF, the posterior distribution of the state is approximated by a number of weighted particles. The PF is suitable for predicting a nonlinear stochastic process with noisy measurements and, thus, has attracted great attentions from both academia and industry [29]-[31]. In the past two decades, the PF has been applied to a variety of applications related to wind energy conversion systems. In [32] and [33], the PF approach was used to optimize the layout of a wind farm to minimize the wake effects and maximize the power generation. In [34], the PF was used to acquire the stator flux of a DFIG, which is an unmeasurable internal state of the DFIG, to enlighten the design of the control scheme. Meanwhile, the PF has also been widely used in the CBM area, such as blade fault diagnosis and prognosis [35], wind turbine drivetrain main bearing [36] and gearbox [37] fault prognosis, and helicopter bearing fault prognosis [38]. Since a wind turbine drivetrain gearbox is a complex system with many components and usually operates under varying conditions, it is hard to obtain an accurate physical degradation model to describe the fault development of the bearings in the gearbox. In [39], an adaptive-neuro-fuzzy-inference-system-based PF (ANFIS-PF) algorithm was proposed for the RUL prediction of wind turbine drivetrain gearboxes. In that PF algorithm, a data-driven model called ANFIS was designed to learn the state transition function of the fault degradation model to remove the need for a physical degradation model. Thus, the ANFIS-PF is a hybrid method that can leverage the strengths of both data-driven and model-based methods and is suitable for the RUL prediction of wind turbine drivetrain gearboxes whose physical degradation models are hard to obtain.

However, the accuracy of the PF methods is limited by the particle impoverishment problem in the resampling procedure. The problem occurs when all but a few particles have negligible weights. As a result, the posterior distribution of the state is inaccurately approximated by a small number of large-weight particles. This problem will reduce the diversity of the particles and, thus, can lead to misleading state estimation results. Several modified PF algorithms have been proposed to solve the particle impoverishment problem. A simple strategy is to rough the overcentralized particles with Gaussian noise [40]. However, that strategy only relies on the resampled particles with large weights. In severe cases, these particles may only have very few distinct values and, thus, provide little improvement of the particle diversity. In [41], the authors proposed a resample-move algorithm to mitigate the particle impoverishment based on the Markov chain Monte Carlo sampling. The Kullback–Leibler Distance (KLD)-sampling [42] and KLD-resampling [43] approaches were proposed to determine the number of particles used in the PF based on the KLD between the actual distribution and the distribution estimated by particles. In [44], an intelligent PF algorithm inspired by the genetic algorithm (GA) was proposed to solve the particle impoverishment problem. However, the GA operators increased the complexity and computational cost of the PF algorithm.

This paper proposes a new particle modification method and an improved multinomial resampling method to solve the particle impoverishment problem in the resampling process of the existing PF algorithms. The particle modification method

modifies the weights of small-weight particles so that they become large-weight ones. Then, the improved multinomial resampling method further increases the diversity of the particles. The proposed particle modification and improved multinomial resampling methods do not increase the computational complexity when compared to the traditional multinomial resampling method. The proposed methods are used for the particle resampling in the PF algorithm, leading to an enhanced PF (EPF) algorithm. Based on the EPF algorithm, a strategy is designed for the continuous RUL prediction of the bearings in wind turbine drivetrain gearboxes to facilitate the CBM to reduce the costs caused by repair and downtime.

The paper is organized as follows. Section II briefly reviews the PF algorithm and discusses the particle impoverishment problem encountered in the PF algorithm. Section III presents the proposed EPF-based RUL prediction strategy. In Section IV, the EPF-based strategy is validated by predicting the RUL of a bearing in the drivetrain gearbox of a 2.5 MW wind turbine in the field. Section V summarizes the paper by some concluding remarks and recommendations for the future work.

II. A Brief Review of the PF Method and Particle Impoverishment Problem

A. Background of the PF Method

In Bayes' theorem, the posterior probability density function (PDF) of the state, which is the fault indicator in the RUL prediction, is constructed based on all available measurements of the state. For a real-world nonlinear system, it is often difficult to obtain the analytic solution of the posterior PDF [45]. To solve this problem, the PF was proposed to approximate the posterior PDF of the state using a set of particles. In the RUL prediction applications, the measurement equation can be simply expressed in the following form [38].

$$z_k = x_k + v_k \tag{1}$$

where x_k and z_k are the actual value and measurement of the state at the time instant k, respectively; and v_k is the estimated measurement noise, which is assumed to follow a Gaussian distribution.

By using the measurements of the state, the PF predicts the state recursively in three main steps: propagate, update, and resample [46].

Propagate: The state of each particle is propagated using an n^{th}-order Markov model, which predicts the trajectory of the state:

$$\hat{x}_{k+1}^i = f_k(\hat{x}_k^i, \hat{x}_{k-1}^i, \cdots, \hat{x}_{k-n+1}^i) + u_k \tag{2}$$

where $\hat{x}_{k+1}^i$ is the state of the i^{th} particle at the time instant k+1; u_k is a Gaussian white noise; f_k represents the nonlinear state transition function in the fault degradation model; and the symbol ^ on top of each variable indicates that it is an estimated or predicted value of the variable.

According to the propagated states $\hat{x}_{k+1}^i$ (i = 1, ···, N) and their current weights, the state at the time instant k+1, $\hat{x}_{k+1}$, can be predicted as follows:

$$\hat{x}_{k+1} = \sum_{i=1}^{N} w_k^i \hat{x}_{k+1}^i \tag{3}$$

where w_k^i is the weight of the i^{th} particle at the time k and N is the number of particles.

Update: When a measurement z_{k+1} becomes available, the weight of each particle is updated according to the importance sampling principle [46]:

$$w_{k+1}^i \propto w_k^i \, p(z_{k+1} \mid \hat{x}_{k+1}^i) \tag{4}$$

where $\propto$ denotes "in proportion to" and $p(z_{k+1} \mid \hat{x}_{k+1}^i)$ is the likelihood function.

Then, the updated weights are normalized as follows.

$$w_{k+1}^i = \frac{w_{k+1}^i}{\sum_i w_{k+1}^i}, \quad i = 1, 2, \cdots, N \tag{5}$$

Thus, the posterior PDF of the state can be approximated by the particles with associated weights as follows:

$$p(x_{k+1} \mid z_{1:k+1}) \approx \sum_{i=1}^{N} w_{k+1}^i \delta(x_{k+1} - \hat{x}_{k+1}^i) \tag{6}$$

where $\delta(\bullet)$ is the Dirac delta function.

Resample: The PF method usually suffers from the problem of particle weights degeneracy after a few iterations, i.e., all but a few particles will have negligible weights. It has been shown in [40] that the weight degeneracy problem is unavoidable. To solve this problem, resampling of particles is usually performed in the PF [47]-[51]. In the resampling process, the states and weights of the selected particles are updated to reduce the discrepancy between the weights of different particles. A widely-used resampling method is called multinomial resampling [40] in which the particles with small weights are eliminated; and new particles (called resampled particles) are created by duplicating the states of the particles with large weights. The weights of all the resampled particles are set to be equal to 1/N. Then, the posterior PDF of the state can be approximated by the resampled particles as:

$$p(x_{k+1} \mid z_{1:k+1}) \approx \frac{1}{N} \sum_{i=1}^{N} N_{k+1}^i \delta(x_{k+1} - \hat{x}_{k+1}^i) \tag{7}$$

where N_{k+1}^i is the number of the resampled particles whose states are equal to $\hat{x}_{k+1}^i$.

B. The Particle Impoverishment Problem

In the multinomial resampling process, if the number of the large-weight particles is much less than that of the small-weight particles, the states of the resampled particles may only share a few distinct values. This will lead to a low diversity of the resampled particles and may cause incorrect state prediction results. Fig. 1 illustrates the weight degeneracy and particle impoverishment problems of the PF algorithm designed to predict a one-dimensional (1D) state variable. Fig. 1(a) shows the posterior PDF of a 1D state variable to be approximated by the particles in the PF algorithm. In Fig. 1(b), the filled circles represent the particles; the radiuses of the circles represent the weights of the particles; and the location of each circle's center represents the state value of the particle. Since the weight degeneracy phenomenon is observed in Fig. 1(b), namely, only a few particles have predominantly large

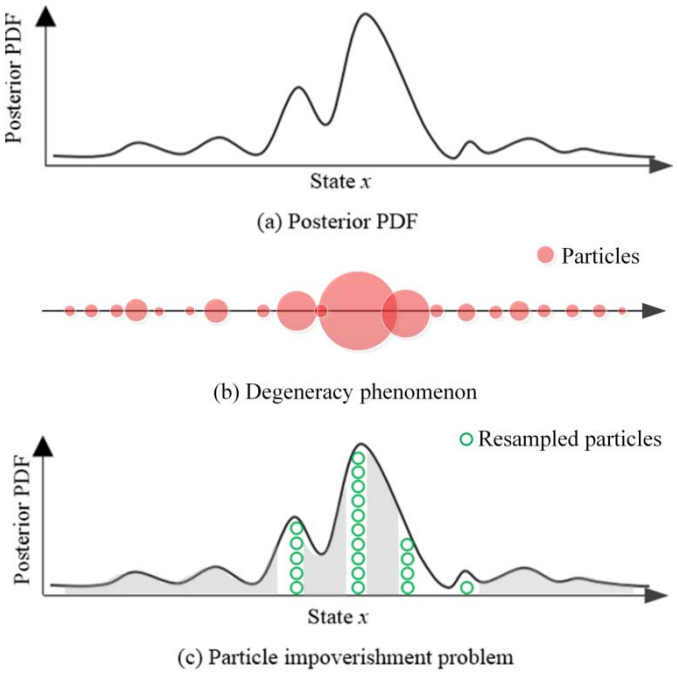

Fig. 1. Illustration of weight degeneracy and particle impoverishment problems in the resampling process: (a) posterior PDF of a 1D state variable, (b) weight degeneracy, and (c) particle impoverishment.

radiuses, resampling is needed. This, however, leads to the particle impoverishment problem as the resampled particles represented by the hollow circles only share a few distinct values, as shown in Fig. 1(c). As a result, the diversity of the resampled particles is reduced compared to the original particles. As shown in Fig. 1(c), the resampled particles cannot approximate the posterior PDF of the state variable accurately because no resampled particles are created within several gray regions with high probabilities. Some literatures have shown that the loss of diversity of the resampled particles will lead to an inaccurate approximation of the posterior distribution of the state and, thus, will have a negative impact on the state prediction results of the PF-based methods [52]-[54]. A straightforward method to solve the impoverishment problem is to increase the number of particles. However, this will increase the computational burden of the PF algorithm significantly. Thus, other computationally efficient methods are desired.

III. Proposed EPF Algorithm for RUL Prediction

This section proposes a new EPF algorithm to predict the RUL of the bearings in DFIG-based wind turbine drivetrain gearboxes. The EPF algorithm solves the particle impoverishment problem in the resampling process of the existing PF algorithms. In the EPF algorithm, a particle modification method is first designed to modify the small-weight particles to become large-weight particles. Thus, more particles have the chance to be selected in the resampling process. Next, an improved multinomial resampling method is proposed to adjust the resampled particles to further increase their diversity.

A. Particle Modification

The effective sample size of particles, N_{eff}, can be regarded as a measure of the dispersion of the weights, which is obtained as follows [28]:

$$N_{eff} = \left[1 / \sum_{i=1}^{N} (w_k^i)^2 \right] \tag{8}$$

where $[\bullet]$ denotes rounding a number. When N_{eff} is less than a fixed threshold N_{thres}, resampling should be performed. The value of N_{thres} can affect the frequency of executing the resampling process. When resampling is required, the particle weights are overcentralized, namely, many particles have small weights and, therefore, contribute little to approximating the posterior distribution of the state. Due to the small number of the large-weight particles with distinct state values, the posterior PDF expressed by (7) is inaccurately approximated, causing a particle impoverishment problem. To solve this problem, the weights of the small-weight particles are increased to obtain more large-weight particles to make the particle weights more even, which implies that the weights of the original large-weight particles will reduce. Therefore, more particles can be selected in the resampling process. In this way, the diversity of the resampled particles will be improved to solve the particle impoverishment problem.

To modify the small-weight particles, the first step is to separate them from the large-weight particles. This is achieved by a particle selection method designed as follows:

$$x_k^i \in \begin{cases} E_l, & w_k^i < W_{th} \\ E_h, & w_k^i \geq W_{th} \end{cases} \tag{9}$$

where E_l and E_h are the sets containing the states of the particles with small and large weights, respectively; and W_{th} is the threshold used for the separation. The weights w_k^i (i = 1, ···, N) of the N particles are sorted in the descending order and stored in $\bar{W}$, i.e.,

$$\bar{W} = \{\bar{w}_k^1, \bar{w}_k^2, \cdots, \bar{w}_k^N\} \tag{10}$$

where $\bar{w}_k^1 \geq \bar{w}_k^2 \geq \cdots \geq \bar{w}_k^N$. Then, the weight of the N_{eff}^{th} particle in $\bar{W}$ is selected as the threshold W_{th}:

$$W_{th} = \bar{W}(N_{eff}) \tag{11}$$

After separating the particles, all the small-weight particles are modified with the help of the large-weight particles; while the large-weight particles remain the same. Let x_{kl}^s be the state of a small-weight particle in E_l to be modified and x_{kh}^t be the state of a large-weight particle in E_h used to help with the modification. Then, the state of a modified small-weight particle, x_{km}^s, is obtained by the linear interpolation as follows:

$$x_{km}^s = \frac{w_{kl}^s \cdot x_{kl}^s + w_{kh}^t \cdot x_{kh}^t}{w_{kl}^s + w_{kh}^t} \tag{12}$$

where w_{kl}^s and w_{kh}^t are the weights of x_{kl}^s and x_{kh}^t stored in $\bar{W}$, respectively; s = 1, ···, N_l; t = 1, ··· , N_h; N_l and N_h are the numbers of particles in E_l and E_h, respectively; and N_h is equal to N_{eff}. For each x_{kl}^s in E_l, x_{kh}^t is randomly selected from E_h. Let X_k' be the set that contains the states of the original large-weight and modified small-weight particles. Then, the weights of the modified small-weight particles in X_k' are updated as:

$$\bar{w}_k^s = \bar{w}_{k-1}^s \frac{1}{\sqrt{2\pi\mu_0}} e^{\frac{-(z_k - x_{km}^s)^2}{2\mu_0}} \quad s = 1, \cdots, N_l \tag{13}$$

where $\bar{w}_{k-1}^s$ is the weight of the modified small-weight particle x_{kl}^s in E_l at the time instant k–1. Then, the weight of the original small-weight particle, w_{kl}^s, stored in $\bar{W}$ is replaced by $\bar{w}_k^s$. Then, normalization is performed as follows for the weights of all the particles stored in $\bar{W}$:

$$\bar{w}_k^i = \frac{\bar{w}_k^i}{\sum_i \bar{w}_k^i}, \quad i = 1, 2, \cdots, N \tag{14}$$

B. Improved Multinomial Resampling

In the traditional multinomial resampling, the states of the resampled particles are simply replicas of the states of the particles with large weights. This may lead to an inaccurately approximation of the posterior distribution of the state variable. Assume that the number of the resampled particles whose states are equal to $x'^i_k \in X'_k$ in the multinomial resampling is N'^i_k. When $N'^i_k > 1$, instead of making N'^i_k copies of x'^i_k, the states of the new resampled particles are generated from x'^i_k in the proposed improved multinomial resampling method and are stored in $\bar{X}_k^i$:

$$\begin{cases} \bar{X}_k^i = \{x^{\bar{w}i}_k, x^{\bar{w}i}_k\}; \ N^{\bar{w}i}_k = 2 \\ \bar{X}_k^i = \{x^{\bar{w}i}_k, x^{\bar{w}i}_k(1 \pm \Delta h^j)\}; j = 1, 2, \cdots, p; N^{\bar{w}i}_k = 2p+1; p > 0 \\ \bar{X}_k^i = \{x^{\bar{w}i}_k, x^{\bar{w}i}_k, x^{\bar{w}i}_k(1 \pm \Delta h^j)\}; j = 1, \cdots, p; N^{\bar{w}i}_k = 2p+2; p > 0 \end{cases} \tag{15}$$

where $\bar{X}_k^i (i = 1, \cdots, N)$ are the sets that contain the states of the new resampled particles generated from x'^i_k; Δh^j is the deviation of the state of a new resampled particle from x'^i_k and is computed as:

$$\Delta h^j = \lambda e^{-\frac{2j-1}{N}}, j = 1, 2, \cdots, \left\lfloor \frac{N^{\bar{w}i}_k - 1}{2} \right\rfloor \tag{16}$$

where λ is used to adjust the decentralization degree of the states of the new resampled particles. To further increase the diversity of the resampled particles such that their states will cover a larger range, the overlap between the states of the new resampled particles should be minimized in the improved multinomial resampling process. Therefore, Δh^1, which represents the largest deviation expressed by (16), should be less than a half of the average minimum difference between the state of each particle, $x'^i_k \in X'_k$ ($i = 1, \cdots, N$), and the states of all other particles $x'^i_k \in X'_k$ ($j = 1, \cdots, N$; $j \neq i$). Thus, the value of λ should satisfy the following:

$$0 < \lambda < \frac{1}{2N} e^{\frac{1}{N}} \sum_{i=1}^{N} \min_{j \neq i} \left(\left| 1 - \frac{x'^j_k}{x^{\bar{w}i}_k} \right| \right) \tag{17}$$

Finally, the states of all of the new resampled particles generated in the improved multinomial resampling process are collected in the set $\bar{X}_k = \{\bar{X}_k^1, \bar{X}_k^2, \cdots, \bar{X}_k^i\}$.

Fig. 2 illustrates the effectiveness of the particle modification and improved multinomial resampling processes in the EPF algorithm. The filled circles with slash lines in purple and red denote the small-weight and large-weight particles, respectively. The filled circles with grid in yellow represent the modified small-weight particles. The solid-line plus dashed-line hollow circles in green represent the resampled particles obtained from the traditional multinomial resampling method; and the solid-line hollow circles in green and purple are the new resampled particles obtained from the proposed improved multinomial resampling method. The radiuses of the circles denote the normalized weights of the

TABLE I:
THE PARTICLE MODIFICATION AND IMPROVED MULTINOMIAL RESAMPLING PROCEDURE IN THE EPF ALGORITHM.

(a) Obtain the particles and their associated weights at the time step k and calculate the effective sample size N_{eff} of particles.
(b) If $N_{eff} < N_{thres}$, resampling is needed.
(c) Sort w_k^i ($i = 1, \cdots, N$) in the descending order and store them in $\bar{W}$.
(d) Set the N_{eff}^{th} weight in $\bar{W}$ as W_{th}.
(e) Divide the particles into small- and large-weight ones and store them in E_l and E_h, respectively.
(f) For $i = 1, 2, \cdots, N_l$
  Implement the particle modification method according to (12) to obtain the states of the modified small-weight particles, and store them together with the states of the large-weight particles in X'_k.
  End
(g) Update and normalize the weights $\bar{w}_k^i$.
(h) Perform the multinomial resampling:
  For $i = 1, 2, \cdots, N$
    Generate a random number y_i from the uniformly distribution over the interval (0, 1];
    Find the variable $j \in \{1, \cdots, N\}$ that satisfies:
$$\sum_{i=1}^{j-1} \bar{w}_k^i < y_i \leq \sum_{i=1}^{j} \bar{w}_k^i \tag{18}$$
    Set x'^i_k as the state of the i^{th} resampled particle; and set the weight of the i^{th} resampled particle as $1/N$.
  End
(i) For $i = 1, 2, \cdots, N$
    Generate the states of new resampled particles $\in \bar{X}_k^i$ according to (15).
  End

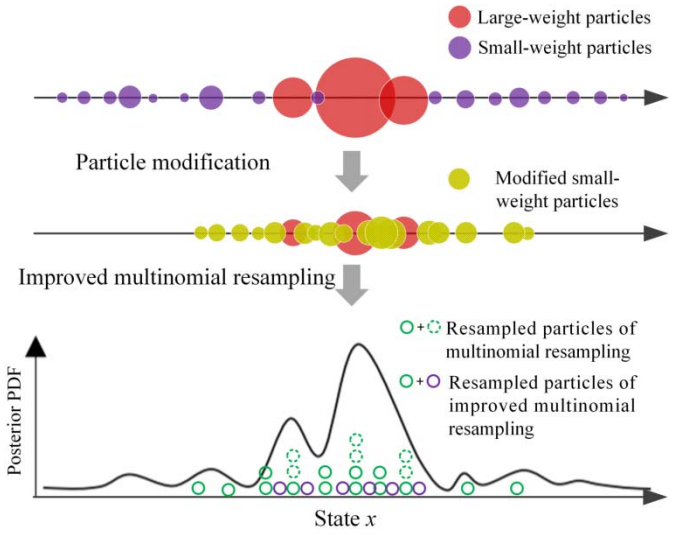

Fig. 2. Illustration of the effectiveness of the particle modification and improved multinomial resampling processes in the EPF algorithm.

corresponding particles. After the particle modification procedure, the normalized weights of the small-weight particles are increased while the normalized weights of the large-weight particles are reduced. Therefore, the normalized weights w'^{i}_{k} of the particles after the modification become more even. Thus, more particles are available for resampling. After applying the improved multinomial resampling method, the diversity of the resampled particles is further increased. Thus, more regions of the posterior PDF of the state variable are covered by the new resampled particles, as shown in Fig. 2. In this way, the particle impoverishment problem can be solved. An implementation of the particle modification and improved multinomial resampling procedures in the EPF algorithm is presented in Table I.

It is important to consider the computational complexity when designing a PF algorithm. The computational complexity of the traditional multinomial resampling method (i.e., Step (h) in Table I) is of an order $O(N\log(N))$ [55]. The $\log(N)$ term arises from the binary search for j in (18). A quicksort algorithm [56] with the computational complexity of an order $O(N\log(N))$ is used to sort w_k^i in the descending order in Step (c) and determine the range of λ in Step (i) of the resampling procedure in the EPF. The computational complexities of the steps (f) and (g) are of orders $O(N_l)$ and $O(N)$, respectively. Therefore, the computational complexities of the particle modification method and the improved multinomial resampling method are both of orders $O(N\log(N))$. Therefore, the total computational complexity of the particle modification and improved multinomial resampling process in the EPF is of an order $O(N\log(N))$, which is the same as the traditional multinomial resampling method. In summary, compared to the traditional multinomial resampling method, the resampling process in the proposed EPF algorithm has a merit of solving the particle impoverishment problem without increasing the computational complexity.

C. RUL Prediction

The RUL is defined as the time between now and the moment when the predicted fault indicator reaches a threshold. If the value of the fault indicator exceeds the threshold, it indicates that the system has failed and can no longer be used, and maintenance should be performed. Since the measurements at future time instants cannot be obtained, it is necessary to predict the future measurements and update the weights of the particles.

During the RUL prediction, the state of each particle is propagated recursively with a fixed state transition function f_k learned by an ANFIS using the latest available measurement:

$$\hat{x}^i_{k+m} = f_k(\hat{x}^i_{k+m-n}, \hat{x}^i_{k+m-n+1}, \cdots, \hat{x}^i_{k+m-1}) + u_k; m = 1, 2, \cdots, T_p \quad (19)$$

where T_p is the prediction period in time steps. Therefore, the predicted measurement at time $k+m$ can be determined by:

$$\hat{z}_{k+m} = \sum_{i=1}^{N} w^i_{k+m-1} \hat{x}^i_{k+m} + v_{k+1} \quad (20)$$

Then, the weights can be updated according to $\hat{z}_{k+m}$:

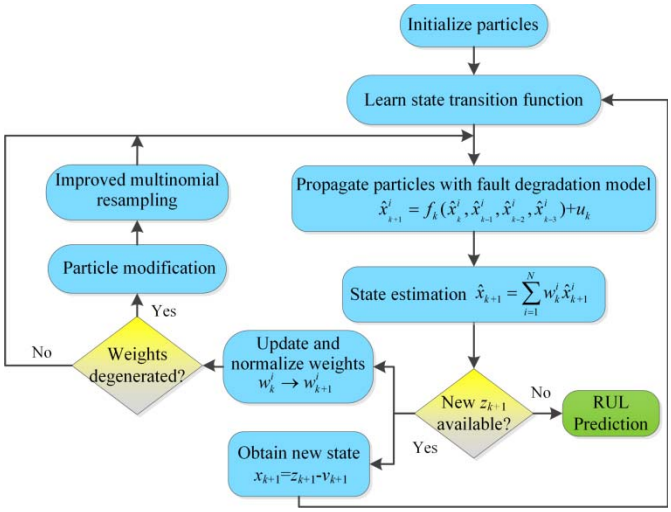

Fig. 3. Flowchart of the EPF-based strategy for the RUL prediction of DFIG-based wind turbine drivetrain gearboxes.

$$w^i_{k+m} = w^i_{k+m-1} \frac{1}{\sqrt{2\pi\mu_0}} e^{\frac{-(\hat{z}_{k+m} - \hat{x}^i_{k+m})^2}{2\mu_0}} \quad (21)$$

Next, the weight normalization is performed as follows:

$$w^i_{k+m} = \frac{w^i_{k+m}}{\sum_i w^i_{k+m}}, \quad i = 1, 2, \cdots, N \quad (22)$$

Thus, the state at $k+m$ can be predicted by:

$$\hat{x}_{k+m} = \sum_{i=1}^{N} w^i_{k+m} \hat{x}^i_{k+m} \quad (23)$$

If the weights degeneracy problem occurs during the RUL prediction, it is necessary to perform resampling. When the state at a future time instant predicted by (23) reaches the threshold, the predicted RUL is determined to be the time between now (i.e., the time instant k) and that future time instant and is denoted as RUL_k.

D. The Overall EPF-Based RUL Prediction Strategy

The flowchart of the overall EPF-based RUL prediction strategy is shown in Fig. 3. The states of all particles are propagated using f_k in the propagate step. When a new measurement is available, the weights of the particles are updated and normalized; and a new value of the state x_{k+1} can be obtained according to (1) and is used to train the ANFIS to learn the state transition function. If the particle weights degeneracy phenomenon occurs, the small-weight particles will be modified to obtain more large-weight particles. Then, the improved multinomial resampling is performed to obtain the resampled particles with a larger diversity. If there is no new measurement, the RUL prediction will be performed. Compared to the widely used multinomial resampling algorithm, the proposed particle modification and improved multinomial resampling methods improve the diversity of the particles by making their weights more even. Thus, the particle impoverishment problem can be solved.

IV. Field Test Validation

The proposed EPF-based RUL prediction strategy is applied to predict the RUL of a bearing in the drivetrain gearbox of a 2.5 MW DFIG wind turbine in the field, which had been operated for approximately five years before maintenance was performed. To show the superior performance of the EPF algorithm, the general PF algorithm with an exponential fault degradation model [37] and the ANFIS-PF algorithm proposed in [39] are used for comparison. A 4th-order Markov model is adopted in the three PF methods. A 4th-order Butterworth low-pass filter is used to smooth the measurements of the fault indicator obtained to improve the learning of the ANFIS.

The RUL of the bearing is predicted repeatedly for $N_s = 30$ times, i.e., 30 experiments. To evaluate the performance of the three PF algorithms, the following two metrics are defined:

$$e_1 = \frac{1}{N_s T_m}\sum_{u=1}^{N_s}\sum_{k=1}^{T_m}\left|z_k - \hat{x}_k^{(u)}\right|,\quad e_2 = \frac{1}{N_s T_p}\sum_{u=1}^{N_s}\sum_{k=T_m+1}^{T_m+T_p}\left|z_k - \hat{x}_k^{(u)}\right| \quad (24)$$

where T_m is the monitoring period in time steps; and $\hat{x}_k^{(u)}$ is the state predicted at the time instant k for the u^{th} experiment. The first metric e_1 is used to evaluate the state estimation result in the monitoring period. During this period, the states of particles of the three PF algorithms are propagated and their weights are updated recursively for the state estimation, i.e., one-step-ahead prediction. Meanwhile, during this period, the ANFISs in the ANFIS-PF and EPF algorithms are trained to obtain their optimal parameters. The second metric e_2 is used to evaluate the RUL prediction result. During the RUL prediction period, no additional monitoring data is available and the RUL prediction is performed with the data collected from the monitoring period only.

The drivetrain gearbox of the 2.5 MW DFIG wind turbine has two planetary stages and one helical stage. The fault indicator is the root mean square (RMS) value of the vibration data recorded from the vibration sensor located on the case of the HSS helical gears. The data was recorded from 10/1/2014 to 11/1/2015 only when the output power is larger than 85% of the rated power. Table II shows some critical time indexes and their corresponding actual time. It should be noted that the time indexes do not increase with the same interval because only part of the data were used.

TABLE II:
Actual Time of Critical Time Indexes.

Time index	Actual time	Time index	Actual time
1600	3/8/2015 22:14:13	2350	3/24/2015 19:53:44
1750	3/17/2015 9:49:54	2680	3/31/2015 16:26:45
1950	3/19/2015 17:49:40	3700	4/21/2015 22:44:38
2050	3/21/2015 1:09:40	4000	4/25/2015 3:15:21
2300	3/23/2015 9:49:28	12170	9/28/2015 7:21:02

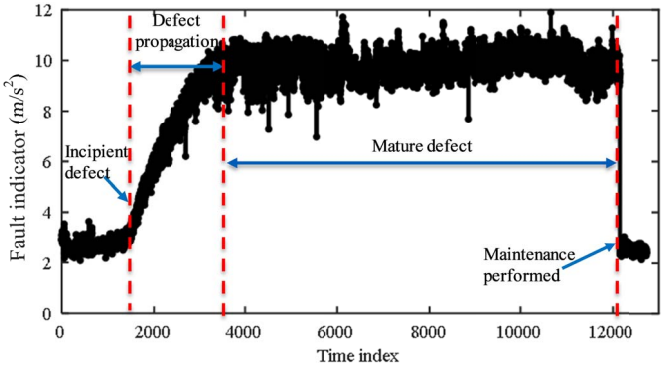

Fig. 4. Extracted fault indicator during the entire data recording period.

Fig. 4 shows the fault indicator extracted during the entire data recording period. The fault indicator increases with the time index during the first 3700 time indexes, indicating that the selected fault indicator is suitable to indicate the fault degradation of the bearing in the gearbox. Meanwhile, it can be observed that the incipient defect occurred around the time index 1600 and the defect propagated from the time index 1600 to 3700. The actual period of the defect propagation was around 45 days. After 3700 time indexes, the defect became mature and the wind turbine still ran normally but a more severe failure that may cause much more cost to repair and longer downtime may happen with a higher probability. The maintenance was performed at the time index 12170 and the fault was found to be an HSS bearing inner raceway ball passing defect inside the gearbox. After the faulty components were replaced, the fault indicator decreased to the normal value rapidly.

The general PF, ANFIS-PF, and proposed EPF algorithms are implemented to perform state estimation and RUL prediction using the same data, where both T_m and T_p are chosen as 2000. The number of particles N in the three PF algorithms is chosen as 100 as a trade-off between prediction accuracy and computational cost. The quantitative evaluation results of the three algorithms are compared in Table III. The general PF and ANFIS-PF algorithms have similar values of e_1, indicating that these two algorithms have the similar state estimation accuracy. However, the ANFIS-PF has a smaller e_2 than the general PF. This is because the ANFIS learned the fault degradation model during the monitoring period, which can significantly reduce the prediction error e_2 in the prediction period. Moreover, the proposed EPF has the smallest e_1 and e_2 among the three algorithms due to the utilization of the proposed particle modification and improved multinomial resampling methods.

The advantages of the proposed EPF are further shown in Fig. 5-7 by comparing with the ANFIS-PF. Fig. 5 compares the values of the fault indicator estimated and predicted by the ANFIS-PF and EPF against the actual values during the entire data recording period, where the first 2000 time indexes are the monitoring period and the two algorithms predict the fault indicator from the time index 2001 to 4000 at the 2000th time index. In the monitoring period, both algorithms can track the trend of the fault indicator well. However, in the prediction period, the fault indicator predicted by the EPF is closer to the actual value than that predicted by the ANFIS-PF. This means that the EPF has a smaller e_2 and, therefore, is more accurate

TABLE III:
Quantitative Evaluation Results of the Three PF Algorithms.

	General PF	ANFIS-PF	EPF
e_1	0.4393	0.4231	0.3645
e_2	2.6426	0.9647	0.6472

for the RUL prediction. The results at the time index k = 551 are selected to further illustrate the effectiveness of the proposed EPF in solving the particle impoverishment problem. At this time index, N_{eff} is smaller than N_{thres}, which is N/4 in this case study. Therefore, resampling is needed. Fig. 6 presents the states and weights of the particles before and after the particle modification. It is obvious that the weights of many particles are small before the modification, and the small-weight particles have little contribution to constructing the posterior PDF of the fault indicator. Since only a small portion of the particles have large weights, the particle diversity is low if the resampling is performed directly, leading to unsatisfactory RUL prediction accuracy. After the particle modification, some of the small-weight particles are modified to become large-weight particles. Therefore, the particle weights become more even and more particles have the potential to be selected in the resampling process. Fig. 7 shows the improvement of the particle diversity using the proposed EPF compared to the ANFIS-PF using the multinomial resampling method. In this paper, λ is chosen as 0.1 according to (17) to adjust the states of the resampled particles in the improved multinomial resampling process of the EPF algorithm. The number of the resampled particles with different state values is 24 when using the ANFIS-PF and increases to 82 when using the EPF, which solves the particle impoverishment problem. Moreover, the number of replicas of the resampled particles is also reduced by adopting the improved multinomial resampling in the proposed EPF.

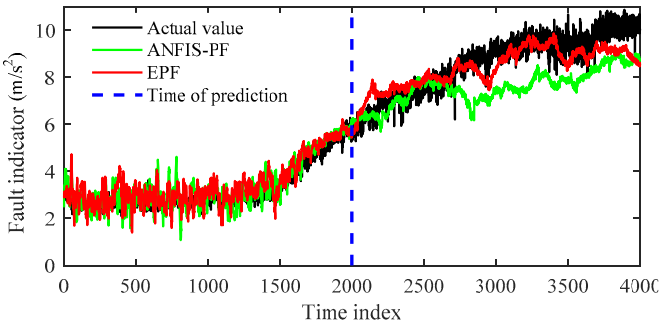

Fig. 5. Fault indicator estimated and predicted by the ANFIS-PF and EPF, where the prediction took place at the time index 2000.

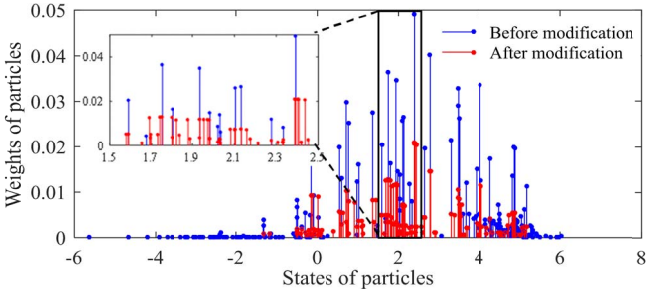

Fig. 6. The particles before and after the particle modification in the EPF at the time index 551.

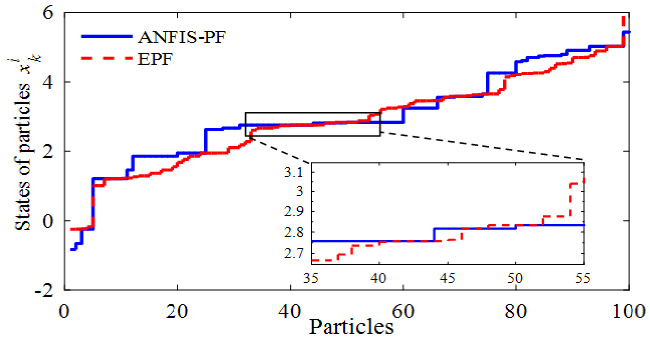

Fig. 7. Particle diversity after resampling when using ANFIS-PF and EPF.

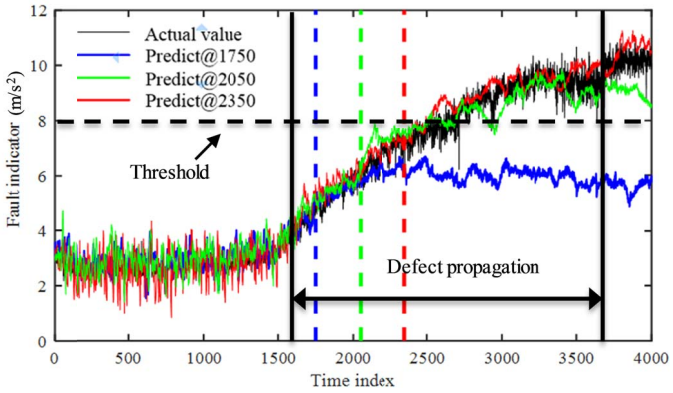

Fig. 8. Fault indicator predicted by the EPF at different time indexes against its actual values.

Fig. 8 compares the fault indicator predicted by the EPF at different time indexes against its actual values. The threshold of the fault indicator was selected to be 8 m/s^2 in this field test validation, which was the same as the threshold used by the vibration-based condition monitoring system of the wind turbine to trigger the fault alarm. When the fault indicator is larger than the threshold, an alarm will be triggered and maintenance can be scheduled in advance to reduce the costs caused by repair and downtime of the wind turbine. The actual fault indicator exceeded 8 m/s^2 at the time index 2680. In Fig. 8, the prediction made at the time index 1750 failed to give the alarm because the predicted fault indicator is always less than the threshold. As time goes on, the predicted value of the fault indicator is closer to the actual value and has a smaller e_2. This is because when more data becomes available, the ANFIS can learn the state transition function better. The prediction made at the time index 2050, which is around 31 days before the defect became mature at the time index 3700, successfully captured the trend of the fault propagation.

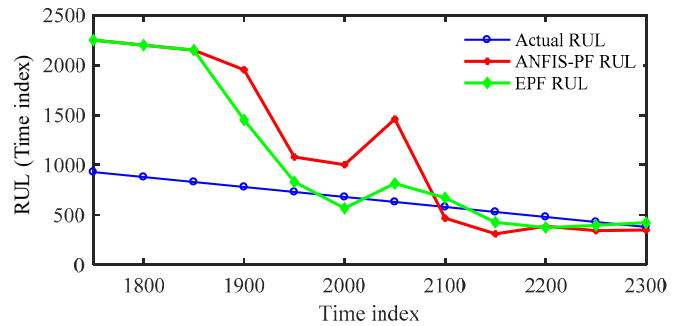

Fig. 9. RUL prediction results of a bearing in a 2.5 WM DFIG wind turbine drivetrain gearbox.

TABLE IV:
COMPARISON BETWEEN THE ACTUAL RUL AND THE RUL PREDICTED BY THE EPF ALGORITHM.

Time index where prediction is performed	Predicted RUL (Time index)	Actual RUL (Time index)	Error time (Days)
1750	2250	930	24.45
1800	2200	880	24.45
1850	2150	830	24.45
1900	1451	780	15.38
1950	831	730	2.08
2000	567	680	-2.32
2050	815	630	3.85
2100	672	580	1.91
2150	427	530	-2.13
2200	374	480	-2.20
2250	396	430	-0.71
2300	423	380	0.89

The ANFIS-PF and EPF are then applied to predict the RUL of the bearing in the wind turbine gearbox every 50 time indexes from the time index 1750 to 2300. Therefore, there are totally 12 RUL prediction cases. The results are shown in Fig. 9 and Table IV. The RUL is defined as the interval between the time at which the prediction is performed and the time at which the fault indicator exceeds the threshold and the alarm is triggered. It should be noted that in some RUL prediction cases, the fault indicator predicted never exceeded the threshold. In these cases, the predicted RUL is set to be the interval between the time at which the RUL prediction starts and the last time step in the prediction period (i.e., the time index 4000). The error time is defined as the predicted RUL minus the actual RUL. A large error time of more than 15 days is observed for the RUL prediction cases from the time index 1750 to 1900 because no enough data is available for training the ANFIS to learn the state transition function f_k in the fault degradation model. Therefore, the RUL prediction in the incipient fault stage leads to a large error time and uncertainty. As the degradation process goes on, more data becomes available to train the ANFIS to learn f_k. Therefore, the error time reduces gradually and the predicted RUL converges to the actual RUL. Compared to the ANFIS-PF, the proposed EPF has less error time. According to Fig. 9 and Table IV, the RUL can be effectively predicted by the EPF with an error time of around 2 days at the time index 1950. This corresponds to the time 17:49:40 on 3/19/2015, which is around 12 days before the actual fault indicator exceeds the threshold. Moreover, after the time index 2250, the error time between the predicted and actual RUL is less than one day.

V. CONCLUSION AND FUTURE WORK

This paper proposed an EPF algorithm for the bearing RUL prediction of DFIG-based wind turbine drivetrain gearbox. In the resampling process of the EPF algorithm, a particle modification method was designed to modify the small-weight particles to obtain more large-weight ones. Thus, more particles could be selected as resampled particles. Then, an improved multinomial resampling method was developed to further increase the diversity of the resampled particles. Thus, the particle impoverishment problem was solved. Compared to the traditional multinomial resampling, the resampling process of the proposed EPF has the same level of computational complexity. Compared with the general PF and ANFIS-PF, the proposed EPF has the best performance in both state estimation and RUL prediction. The effectiveness and superiority of the proposed EPF algorithm for the RUL prediction of the bearings in drivetrain gearboxes were verified using vibration data recorded from a 2.5 MW DFIG-based wind turbine in the field.

A challenge in the RUL prediction is the uncertainty of the prediction results. In the future work, the robustness of the EPF algorithm will be further studied. An outer correction loop [57] and sliding mode control techniques [58]-[60] can be possible solutions to manage the uncertainty and improve the robustness of the EPF algorithm. Moreover, the effectiveness of the EPF algorithm is influenced by the decentralization parameter λ in (17). In this paper, the value of λ is tuned by trial and error within the range determined by (17). In the future work, further improvement could be made by designing an adaptive strategy to tune λ automatically.

REFERENCES

[1] J. Ribrant, "Reliability performance and maintenance, a survey of failures in wind power systems," *Master's Thesis*, KTH, Stockholm, Sweden, 2005–2006.

[2] Y. Feng, Y. Qiu, C. J. Crabtree, H. Long, and P. J. Tavner, "Monitoring wind turbine gearboxes," *Wind Energy*, vol. 16, no. 5, pp. 728–740, July 2013.

[3] B. Lu, Y. Li, X. Wu, and Z. Yang, "A review of recent advances in wind turbine condition monitoring and fault diagnosis," in *Proc. IEEE Power Electron. Mach. Wind Appl*., June 2009, pp. 1–7.

[4] S. Sheng and P. Veers, "Wind turbine drivetrain condition monitoring—An overview," NREL, Golden, CO, USA, Tech. Rep. NREL/CP-5000-50698, May 2011.

[5] S. Sheng, H. Link, W. LaCava,J. van Dam, B. McNiff,P. Veers,J. Keller, S.Butterfield, and F. Oyague, "Wind turbine drivetrain condition monitoring during GRC phase 1 and phase 2 testing," NREL,Tech. Rep. No. TP-5000-52748, Oct. 2011.

[6] S. Sheng, "Gearbox typical failure modes, detection, and mitigation methods," Nat. Renew. Energy Lab., Golden, CO, Tech. Rep. NREL/PR-5000-60982, Jan. 2014.

[7] P. Zhang and P. Neti, "Detection of gearbox bearing defects using electrical signature analysis for doubly fed wind generators," *IEEE Trans. Ind. Appl.*, vol. 51, no. 3, pp. 2195-2200, May./June 2015.

[8] W. Qiao and D. Lu, "A survey on wind turbine condition monitoring and fault diagnosis−Part I: Components and subsystems," *IEEE Trans. Ind. Electron.*, vol. 62, no. 10, pp. 6536-6545, Oct. 2015.

[9] W. Qiao and D. Lu, "A survey on wind turbine condition monitoring and fault diagnosis−Part II: Signals and signal processing methods," *IEEE Trans. Ind. Electron.*, vol. 62, no. 10, pp. 6546-6557, Oct. 2015.

[10] Y. Lei, J. Lin, M. J. Zuo, and Z. He, "Condition monitoring and fault diagnosis of planetary gearboxes: A review," *Measurement*, vol. 48, pp. 292–305, Feb. 2014.

[11] Z. Hameed, Y. S. Hong, Y. M. Cho, S. H. Ahn, and C. K. Song, "Condition monitoring and fault detection of wind turbines and related algorithms: A review," *Renew. Sustain. Energy Rev*., vol. 13, no. 1, pp. 1–39, Jan. 2009.

[12] F. Cheng, Y. Peng, L. Qu, and W. Qiao, "Current-based fault detection and identification for wind turbine drivetrain gearboxes," *IEEE Trans. Ind. Appl.*, vol. 53, no. 2, pp. 878-887, Mar.-Apr. 2017.

[13] F. Cheng, C. Wei, L. Qu, and W. Qiao, "Fault diagnosis of wind turbine gearbox using DFIG stator current analysis," in *Proc. IEEE Energy Convers. Congr. Expo.,* Sept. 2016, pp. 1-7.

[14] X. Jin, F. Cheng, Y. Peng, W. Qiao and L. Qu, "A comparative study on Vibration- and current-based approaches for drivetrain gearbox fault diagnosis," in *Proc. 51st IEEE Ind. Appl. Soc. Annu. Meeting*, Oct. 2016, pp. 1-8.

[15] L. Wang, Z. Zhang, H. Long, J. Xu, and R. Liu, "Wind turbine gearbox failure identification with deep neural network," *IEEE Trans. Ind. Informat.*, vol. 13, No. 3, pp. 1360-1368, Jun. 2017.

[16] Z. Zhang, A. Verma, and A. Kusiak, "Fault analysis of the wind turbine gearbox," *IEEE Trans. Energy Convers.*, vol. 27, No. 2, pp. 526-535, Jun. 2012.

[17] G. Jiang, H. He, P. Xie, and Y. Tang, "Stacked multilevel-denoising autoencoders: A new representation learning approach for wind turbine gearbox fault diagnosis," *IEEE Trans. Instrum. and Meas.*, vol. 66, no. 9, pp. 2391-2402, Sept. 2017.

[18] F. Cheng, J. Wang, L. Qu, and W. Qiao, "Rotor-current-based fault diagnosis for DFIG wind turbine drivetrain gearboxes using frequency analysis and a deep classifier," *IEEE Trans. Ind. Appl.*, vol. 54, no. 2, pp. 1062-1071, Mar.-Apr. 2018.

[19] J. Wang, F. Cheng, W. Qiao, and L. Qu, "Multiscale filtering reconstruction for wind turbine gearbox fault diagnosis under varying-speed and noisy conditions," *IEEE Trans. Ind. Electron.*, vol. 65, no. 5, pp. 4268-4278, May 2018.

[20] Z. Gao, C. Cecati, and S. X. Ding, "A survey of fault diagnosis and fault-tolerant techniques—Part I: Fault diagnosis with model-based and signal-based approaches," *IEEE Trans. Ind. Electron.,* vol. 62, no. 6, pp. 3757–3767, June 2015.

[21] J. Luo, A. Bixby, K. Pattipati, L. Qiao, M. Kawamoto, and S. Chigusa, "An interacting multiple model approach to model-based prognostics," in *Proc. IEEE Int. Conf. Syst., Man, Cybern*., vol. 1, Oct. 2003, pp.189-194.

[22] Y. Li, T. R. Kurfess, and S. Y. Liang, "Stochastic prognostics for rolling element bearings," *Mech. Syst. Signal Process.*, vol. 14, no. 5, pp. 747-762, Sept. 2000.

[23] D. Tobon-Mejia, K. Medjaher, N. Zerhouni, and G. Tripot, "A data-driven failure prognostics method based on mixture of Gaussians hidden Markov models," *IEEE Trans. Rel.*, vol. 61, no. 2, pp. 491–503, June 2012.

[24] F. Yang, M. S. Habibullah, T. Zhang, Z. Xu, P. Lim, and S. Nadarajan, "Health index-based prognostics for remaining useful life predictions in electrical machines," *IEEE Trans. Ind. Electron*., vol. 63, no. 4, pp. 2633–2644, Apr. 2016.

[25] S. Yin, G. Wang, and X. Yang "Robust PLS approach for KPI-related prediction and diagnosis against outliers and missing data," *Int. J. Syst. Sci.*, vol. 45, no. 7, pp. 1375–1382, Feb. 2014.

[26] R. Huang, L. Xi, X. Li, C. R. Liu, H. Qiu, and J. Lee, "Residual life predictions for ball bearings based on self-organizing map and back propagation neural network methods," *Mech. Syst. Signal Process.*, vol. 21, no. 1, pp. 193–207, Jan. 2007.

[27] Z. Gao, C. Cecati, and S. X. Ding, "A Survey of fault diagnosis and fault-tolerant techniques part II: Fault diagnosis with knowledge-based and hybrid/active approaches," *IEEE Trans. Ind. Electron.*, vol. 62, no. 6, pp. 3768–3774, June 2015.

[28] A. Doucet, S. Godsill, and C. Andrieu, "On sequential Monte Carlo sampling methods for Bayesian filtering," *Statist. Comput*., vol. 10, no. 3, pp. 197–208, July 2000.

[29] F. Gustafsson *et al.*, "Particle filters for positioning, navigation, tracking," *IEEE Trans. Signal Process.*, vol. 50, no. 2, pp. 425–437, Feb. 2002.

[30] A. Shenoy, J. Prakash, V. Prasad, S. Shah, and K. McAuley, "Practical issues in state estimation using particle filters: Case studies with polymer reactors," *J. Process Control*, vol. 23, no. 2, pp. 120–131, Feb. 2013.

[31] S. Das, A. Kale, and N. Vaswani, "Particle filter with a mode tracker for visual tracking across illumination changes," *IEEE Trans. Image Process.*, vol. 21, no. 4, pp. 2340–2346, Apr. 2012.

[32] Y. Eroğlu and S. U. Seçkiner, "Wind farm layout optimization using particle filtering approach," *Renew. Energy*, vol. 58, pp. 95-107, Oct. 2013.

[33] P. A. Fleming, P. M. O. Gebraad, M. J. Churchfield, J. W. van Wingerden, A. K. Scholbrock, and P. J. Moriarty, "Using particle filters to track wind turbine wakes for improved wind plant controls," in *Proc. American Control Conf.*, Jun. 2014, pp. 3734-3741.

[34] S. Yu, T. Fernando, H. H. C. Iu, and K. Emami, "Realization of state-estimation-based DFIG wind turbine control design in hybrid power systems using stochastic filtering approaches," *IEEE Trans. Ind. Informat.*, vol. 12, no. 3, pp. 1084-1092, Jun. 2016.

[35] M. Orchard and G. Vachtsevanos, "A particle filtering approach for on-line fault diagnosis and failure prognosis," *Trans. Inst. Meas. Control*, vol. 31, no. 3/4, pp. 221–246, June 2009.

[36] S. Sharma and D. Mahto, "Condition monitoring of wind turbine gear-box," *Int. J. Res. Studies Sci., Eng. Technol.*, vol. 1, no. 5, pp. 33–51, Aug. 2014.

[37] X. Fan, X. Yang, X. Li, and J. Wang, "A particle-filtering approach for remaining useful life estimation of wind turbine gearbox," in *Proc. Int. Conf. Chemical Material and Food Eng.*, Jan. 2015, pp. 198-200.

[38] C. Chen, B. Zhang, G. Vachtsevanos, and M. Orchard, "Machine condition prediction based on adaptive neuro–fuzzy and high-order particle filtering," *IEEE Trans. Ind. Electron*., vol. 58, no. 9, pp. 4353–4364, Sept. 2011.

[39] F. Cheng, L. Qu, and W. Qiao, "Fault prognosis and remaining useful life prediction of wind turbine gearboxes using current signal analysis," *IEEE Trans. Sustain. Energy*, vol. 9, no. 1, pp. 157-167, Jan. 2018.

[40] N. J. Gordon, D. J. Salmond, and A. F. Smith, "Novel approach to nonlinear/non-Gaussian Bayesian state estimation," *Proc. Inst. Elect. Eng.—Radar Signal Process*., vol. 140, no. 2, pp. 107–113, Apr. 1993.

[41] W. R. Gilks and C. Berzuini, "Following a moving target-Monte Carlo inference for dynamic Bayesian models," *J. Roy. Stat. Soc. B.*, vol. 63, no. 1, pp. 127–146, 2001.

[42] D.Fox, "Adapting the sample size in particle filters through KLD-sampling," *Int. J. Robot. Res*., vol. 22, no. 12, pp. 985-1003, Dec. 2003.

[43] T. Li, S. Sun, and T. P. Sattar, "Adapting sample size in particle filters through KLD-resampling," *Electron. Lett*., vol. 49, no. 12, pp. 740–742, June 2013.

[44] S. Yin and X. Zhu, "Intelligent particle filter and its application to fault detection of nonlinear systems," *IEEE Trans. Ind. Electron*., vol. 62, no. 6, pp. 3852–3861, June 2015.

[45] C. Chen, B. Zhang, and G. Vachtsevanos, "Prediction of machine health condition using neuro-fuzzy and Bayesian algorithms," *IEEE Trans. Instrum. Meas*., vol. 61, no. 2, pp. 297–306, Feb. 2012.

[46] M. S. Arulampalam, S. Maskell, N. Gordon, and T. Clapp, "A tutorial on particle filters for online nonlinear/non-Gaussian Bayesian tracking," *IEEE Trans. Signal Process.*, vol. 50, no. 2, pp. 174–188, Feb. 2002.

[47] F. Cheng, L. Qu, and W. Qiao, "A case-based data-driven prediction framework for machine fault prognostics," in *Proc. Energy Convers. Congr. Expo.*, Sept. 2015, pp. 3957-3963.

[48] T. Higuchi, "Monte Carlo filter using the genetic algorithm operators," *J. Stat. Comput. Simul*., vol. 59, no. 1, pp. 1–23, Aug. 1997.

[49] T. Li, M. Bolic, and P. M. Djuric, "Resampling methods for particle filtering," *IEEE Signal Process. Mag*., vol. 32, no. 3, pp. 70–86, May 2015.

[50] S. M. K. Heris and H. Khaloozadeh, "Non-dominated sorting genetic filter a multi-objective evolutionary particle filter," in *Proc. Iranian Conf. Intell. Syst*., 2014, pp. 1–6.

[51] R. Douc and O. Cappé, "Comparison of resampling schemes for particle filtering," in *Proc. Intell. Symp. Image Signal Process. Anal*., Jul. 2005, pp. 64–69.

[52] S. Lee, J. Kang, and S. Lee, "Enhanced particle-filtering framework for vessel segmentation and tracking", *Computer Methods and Programs in Biomedicine*, vol. 148, pp. 99-112, Sept. 2017.

[53] N. M. Kwok, G. Fang, and W. Zhou, "Evolutionary particle filter: Re-sampling from the genetic algorithm perspective," in *Proc. IEEE/RSJ Int. Conf. Intell. Robots Syst.*, Aug. 2005, pp. 2935–2940.

[54] S. Yin, X. P. Zhu, J. B. Qiu, and H. J. Qiu, "State estimation in nonlinear system using sequential evolutionary filter," *IEEE Trans. Ind. Electron*., vol. 63, no. 6, pp. 3786–3794, Jun. 2016.

[55] J. Carpenter, P. Clifford, and P. Fearnhead, "Improved particle filter for nonlinear problems," *Proc. Inst. Elect. Eng., Radar, Sonar, Navig*., vol. 146, no. 1, pp. 2-7, Feb. 1999.

[56] C. A. R. Hoare, "Algorithm 64: Quicksort," *Commun. ACM*, vol. 4, no. 7, pp. 321, Jul. 1961.

[57] M. Orchard, G. Kacprzynski, K. Goebel, B. Saha, and G. Vachtsevanos, "Advances in uncertainty representation and management for particle filtering applied to prognostics," in *Proc. Int. Conf. Prognostics and Health Manag*., Oct. 2008, pp. 1-6.

[58] Y. Wang, Y. Gao, H. R. Karimi, H. Shen, and Z. Fang, ''Sliding mode control of fuzzy singularly perturbed systems with application to electric circuits,'' *IEEE Trans. Syst. Man, Cybern. Syst*., to be published, doi: 10.1109/TSMC.2017.2720968.

[59] Y. Wang, H. Shen, H. R. Karimi, and D. Duan, ''Dissipativity-based fuzzy integral sliding mode control of continuous-time T-S fuzzy systems,'' *IEEE Trans. Fuzzy Syst*., to be published, doi: 10.1109/TFUZZ.2017.2710952.

[60] Y. Wang, Y. Xia, H. Shen, and P. Zhou, "SMC design for robust stabilization of nonlinear Markovian jump singular systems," *IEEE Trans. Autom. Control*, vol. 63, no. 1, pp. 219-224, Jan. 2018.

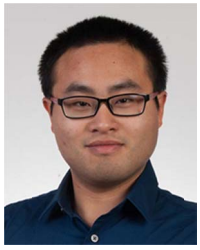

Fangzhou Cheng (S'15–M'18) received the B.Eng. degree in electrical engineering from Zhejiang University, Hangzhou, China, in 2013, and the Ph.D. degree in electrical engineering from the University of Nebraska–Lincoln, Lincoln, NE, USA, in 2017.

He is currently a Data Scientist with the System Sciences Laboratory, Palo Alto Research Center (PARC), CA, USA. His research interests include renewable energy systems, machine learning, condition-based maintenance, and intelligent fault diagnosis and prognosis for various cyber-physical systems.

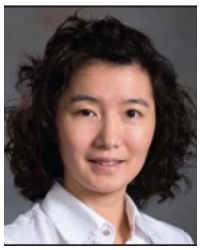

Liyan Qu (S'05–M'08–SM'17) received a B.Eng. (with the highest distinction) and an M.Eng. degrees in electrical engineering from Zhejiang University, Hangzhou, China, in 1999 and 2002, respectively, and a Ph.D. degree in electrical engineering from the University of Illinois at Urbana–Champaign, Champaign, IL, USA, in 2007.

From 2007 to 2009, she was an Application Engineer with Ansoft Corporation, Irvine, CA, USA. Since January 2010, she has been with the University of Nebraska−Lincoln, Lincoln, NE, USA, where she is currently an Associate Professor with the Department of Electrical and Computer Engineering. Her research interests include energy efficiency, renewable energy, numerical analysis and computer aided design of electric machinery and power electronic devices, dynamics and control of electric machinery, and magnetic devices.

Dr. Qu was a recipient of the 2016 U.S. National Science Foundation CAREER Award.

Wei Qiao (S'05–M'08–SM'12) received a B.Eng. and an M.Eng. degrees in electrical engineering from Zhejiang University, Hangzhou, China, in 1997 and 2002, respectively, an M.S. degree in high-performance computation for engineered systems from Singapore-MIT Alliance, Singapore, in 2003, and a Ph.D. degree in electrical engineering from Georgia Institute of Technology, Atlanta, GA, USA, in 2008.

Since August 2008, he has been with the University of Nebraska–Lincoln, Lincoln, NE, USA, where he is currently a Professor with the Department of Electrical and Computer Engineering. His research interests include renewable energy, smart grids, condition monitoring, power electronics, electric machines and drives, and new electrical energy conversion devices. He is the author or coauthor of more than 220 papers in refereed journals and conference proceedings.

Dr. Qiao is an Editor of the IEEE TRANSACTIONS ON ENERGY CONVERSION and the IEEE POWER ENGINEERING LETTERS, and an Associate Editor of the IEEE TRANSACTIONS ON POWER ELECTRONICS and the IEEE JOURNAL OF EMERGING AND SELECTED TOPICS IN POWER ELECTRONICS. He was the recipient of a 2010 U.S. National Science Foundation CAREER Award and the 2010 IEEE Industry Applications Society Andrew W. Smith Outstanding Young Member Award.

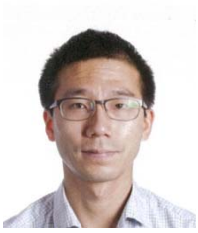

Liwei Hao (S'06–M'08–SM'14) received the B.Eng. degree in electrical engineering and automation from the Xi'an Jiaotong University, Xi'an, China, in 2004 and the Ph.D. degree in electrical engineering from the University of Southampton, Southampton, U.K., in 2008.

He worked as a Research Fellow in the Tony Davies High Voltage Laboratory, University of Southampton, U.K., where he was involved in numerous high voltage and condition monitoring projects for electrical power and grid applications. He joined GE Global Research, Niskayuna, NY, USA, in 2012 as a Lead Electrical Engineer and is currently a Technical Operations Leader at the center. He has been leading different projects cross a wide range of GE businesses including power, transportation, oil and gas, energy connections, renewable energy, fuel cells, ventures, and government funded programs. His research interests and experience include condition monitoring, diagnostics and prognostics for electrical power assets, high voltage AC and DC component and system design, applied signal processing and digital twin for various grid and industrial applications, industrial internet, big data analytics, and artificial intelligence for electric power and industrial systems.